A NEW CONFORMAL MAPPING TECHNIQUE FOR SHIP SECTIONS

P. C. Westlake and P. A. Wilson

*Department of Ship Science,*
*University of Southampton, Southampton, U.K.*

*Int. Shipbuild. Progr.,* ??, no. ??? (1998) pp.???-???

*Received : April 1998*
*Accepted : September 1998*

A multiparameter conformal mapping technique is presented which permits the accurate description of realistic ship sections. The solution of a nonlinear set of equations describing the transformation of a circle to the arbitrarily shaped section is linearised using a new method which produces a monotonic relationship between coordinates in the physical and reference planes. This feature allows the mapping of reentrant sections such as large bulbous bows and the inclusion of features such as bilge keels and shaft brackets. The assumed form of the conformal mapping permits asymmetric sections to be represented. The sections can be successfully transformed at different heel angles.

# 1 Introduction.

The prediction of ship response in a realistic seaway and the estimation of wave loadings are some of the most important aspects of ship design. The wave induced motions are capable of making the ships intended roles impossible, whilst extreme wave loadings may have catastrophic consequences. The accurate prediction of these quantities at the design stage, until recently, relied on model tests which may not be immediately available or desirable.

A realistic seaway may be represented by the summation of unidirectional sinusoidal waves and under the assumptions of linear theory, the ship response to the irregular sea may be determined from the responses to each unidirectional component as described by St Denis and Pierson(1953). Thus the ship seakeeping problem reduces to the prediction of the response of a ship in a regular wave system.

The equations describing the rigid body ship motions in the six possible degrees of freedom are second order differential equations whose coefficients are required in order to obtain the motion responses. The *mass* term consists of the real mass (or first or second moment) plus the added mass (or added inertia), this is referred to as the virtual mass. The added mass term represents the mass of fluid surrounding the ship that is also accelerated with the ship. The *damping*

term represents the energy lost due to wave generation on the free surface due to the motions of the ship. The *stiffness* term represents the hydrostatic restoring forces acting on the ship due to the inbalance of buoyancy and weight. The six equations are, in general, coupled together, that is, a displacement in one mode of motion will produce a force/moment in a different mode and vice versa. For instance, an asymmetric body experiencing heave will generate a sway force. Therefore, in general, there are thirty six forms of each coefficient, although under conditions of lateral symmetry many of these elements are zero, see Price and Bishop(1974).

Therefore to obtain a prediction of a ship response in a regular wave system requires the accurate estimation of the coefficients of the differential equations. The derivation of the added mass and damping coefficients present significant difficulties compared with other required terms. Strip theory simplifications reduce the determination of the added mass and damping coefficients to a two dimensional problem, see Salvesen et al(1970). The coefficients are determined for a number of longitudinal sections swaying, heaving and rolling harmonically at the frequency of the incident wave in the free surface. A consequence of strip theory assumptions is that the response calculated for each section is independent of the disturbance created by other sections. The coefficients for the entire ship are then obtained by integration.

The two dimensional coefficients are obtained using a potential flow solution, the form of which is selected to satisfy Laplace's equation, the free surface and radiation conditions. The solution is composed of the linear combination of a source and multipole potentials, the strengths of the multipoles being used to enforce the boundary conditions on the body perimeter. Ursell(1949a,b) derives the potential for a cylinder heaving and rolling in the free surface. The extension of this method to elliptic, Lewis and arbitrarily shaped sections are described by Wehausen(1971). Count(1977a,b) derives the velocity potential for an asymmetric section which is utilised by Conceição et al(1984) to study the effects of heel on the added mass and damping coefficients. Kobayashi(1975) uses a different technique to examine the stability of heeled ships in beam seas.

The form of the multipole potential selected to satisfy the boundary conditions on the perimeter of the arbitrarily shaped section contains coefficients used in a conformal mapping which transforms the section in the physical plane to a unit circle in the reference plane. This situation arises because the form of the multipole potential used to represent the boundary conditions on the perimeter of a circle is no longer applicable to the arbitrarily shaped section. A conformal mapping is utilised to transform the section into a circle, for which the form of the multipole potential is known. This representation is then transformed back into the physical plane using the derived mapping.

The problem now becomes one of determining the parameters in the transformation which map the arbitrary section to a unit circle. The earliest mapping using two parameters is due to Lewis(1929), these produce reasonable representations of conventional sections but are unsuitable for very fine or full

sections. Complex and reentrant sections may not be represented. Analytical expressions for the added mass and damping coefficients exist. Landweber and Macagno(1959) extended the transformation to three parameters and generalised to N parameters, see Landweber and Macagno(1957). A bibliography of conformal transformation techniques is provided in Conceição et al(1984) and the various methods which exist to obtain the transform parameters are discussed by Bishop et al(1979).

## 2 The conformal mapping technique.

The problem is posed with respect to Figure 1 where we locate the origin of a rectangular coordinate system in the physical plane on the undisturbed free surface. The $x$ axis is horizontal, the $y$ axis is positive downward. The angle $\phi$ is defined to be positive anticlockwise from the positive $y$ axis. The arbitrarily shaped body is defined by $P$ points, the first point located on the positive $x$ axis, the definition proceeding clockwise.

In the reference plane the origin is located at the centre of the unit circle on the horizontal $\xi$ axis. The $\eta$ axis is positive vertically downward. The angle $\theta$ is defined to be positive anticlockwise from the positive $\eta$ axis. Using a conformal mapping, $z = f(\zeta)$, the points $(1, \theta_p)$ in the $\zeta$ plane are mapped to the points $(x_p, y_p)$ in the $z$ plane.

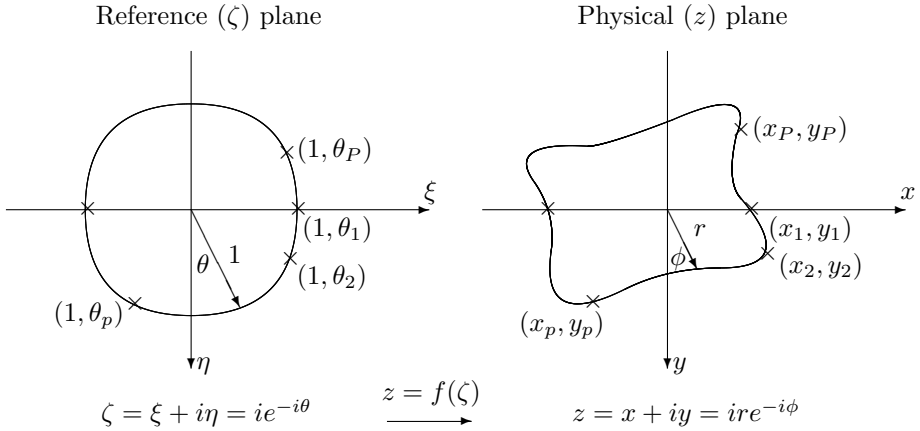


Figure 1: Coordinate systems in the reference and physical planes.

The form of a suitable transformation mapping an arbitrarily shaped section to a unit circle is now discussed.

## 2.1 The multiparameter transformation.

An appropriate mapping takes the form, see de Jong(1973),

$$z = x + iy = ire^{-i\phi} = \sum_{n=-1}^{n=\infty} c_n \zeta^{-n} \tag{1}$$

where $c_n$ are the complex transformation parameters, $c_n = a_n + ib_n$.

As this analysis is only concerned with the region $y \geq 0$ the transformation may be simplified by assuming the $x$ axis is a line of symmetry and the point $(x_P, y_P)$ is now located on the negative $x$ axis. The symmetry relation is

$$z(\zeta) = \overline{z(\bar{\zeta})} \tag{2}$$

where the overline indicates a conjugate operator. Using this relationship it can be easily shown that the terms $b_n$, $n = -1, 0, 1, 2...$ are zero. The transformation may then be expressed as

$$\begin{aligned} x &= a\sin\theta + \sum_{n=0}^{n=\infty} (-1)^n [a_{2n}\cos 2n\theta + a_{2n+1}\sin(2n+1)\theta] \\ y &= a\cos\theta + \sum_{n=0}^{n=\infty} (-1)^n [a_{2n}\sin 2n\theta - a_{2n+1}\cos(2n+1)\theta] \end{aligned} \tag{3}$$

where the term $a_{-1}$ is renamed $a$ and referred to as the scale factor. When the ship section is circular the parameters $a_{2n}$ and $a_{2n+1}$, $n = 0, 1, 2...$ are zero and only the scale factor is used to size the mapping.

When the ship sections are symmetric about the centreplane a further simplification may be applied. This symmetry relation has the form

$$z(\zeta) = -\overline{z(-\bar{\zeta})} \tag{4}$$

Applying this condition in conjunction with the condition specified in equation 2 the parameters $a_{2n}$ are zero and transformation reduces to

$$\begin{aligned} x &= a\sin\theta + \sum_{n=0}^{n=\infty} (-1)^n a_{2n+1}\sin(2n+1)\theta \\ y &= a\cos\theta + \sum_{n=0}^{n=\infty} (-1)^{n+1} a_{2n+1}\cos(2n+1)\theta \end{aligned} \tag{5}$$

When the upper limit of the summation is reduced to unity the formulation becomes the Lewis transformation.

## 2.2 The Lewis transformation.

For a symmetric section the Lewis mapping may be applied to approximate ship shaped sections. The transformation has the form, see Lewis(1929),

$$z = x + iy = ire^{-i\phi} = a\zeta + \frac{a_1}{\zeta} + \frac{a_3}{\zeta^3} \tag{6}$$

where the transform parameters are given by

$$\begin{gathered} a_1 = \tfrac{1}{2}(b-t) \\ a_3 = \tfrac{1}{4}\left[-(b+t) + \sqrt{\left|(b+t)^2 + 8(bt - \tfrac{4A}{\pi})\right|}\right] \\ a = \tfrac{1}{2}(b+t) - a_3 \end{gathered} \tag{7}$$

where $b$ is the sectional half beam, $t$ is the sectional draught and $A$ is the submerged area of the section. Mapping are only possible in the regions

$$\begin{array}{ll} \frac{3\pi}{32}(2-\lambda) \le \sigma \le \frac{3\pi}{32}(3+\frac{1}{4\lambda}) & \lambda < 1 \\ \frac{3\pi}{32}(2-\frac{1}{\lambda}) \le \sigma \le \frac{3\pi}{32}(3+\frac{\lambda}{4}) & \lambda \ge 1 \end{array} \tag{8}$$

where $\sigma = \frac{A}{2bT}$ and $\lambda = \frac{b}{T}$. Sections outside of these ranges will not produce suitable mappings as illustrated by von Kerczek and Tuck(1969) and it is usual practice to use the nearest limit of the inequalities to produce a valid mapping.

## 2.3 Implementation of the mapping.

Normally the definition of a ship section takes the form of a set of discrete points $(x_p, y_p), p = 1..P$. At each definition point in the $z$ plane there exist a corresponding unknown angle $\theta_p$ in the $\zeta$ plane which must be determined. Two angles however are known at the outset, these correspond to the points on the waterline. These are

$$\begin{gathered} x_1 = b_s \text{ at } \theta = \tfrac{\pi}{2} \\ x_P = -b_p \text{ at } \theta = -\tfrac{\pi}{2} \end{gathered} \tag{9}$$

where $b_p$ and $b_s$ are the port(left) and starboard(right) waterline offsets. Therefore there are $P-2$ unknown angles.

In practice the summation present in the conformal conformal mapping given by equation 3 is truncated at a suitable upper limit $N$ and the total number of unknown transform parameters is $2N+3$. Each definition point provides two equations except at the waterline where $y = 0$, therefore the problem is only solvable if the number of points, P, used to define the section is greater than or equal to $2N+3$. Usually, the number of definition points exceeds this figure and the problem is solved in a least square sense. Equation 3 becomes

$$\left.\begin{aligned} x_p &= a\sin\theta_p + \sum_{n=0}^{n=N}(-1)^n[a_{2n}\cos 2n\theta_p + a_{2n+1}\sin(2n+1)\theta_p] \\ y_p &= a\cos\theta_p + \sum_{n=0}^{n=N}(-1)^n[a_{2n}\sin 2n\theta_p - a_{2n+1}\cos(2n+1)\theta_p] \end{aligned}\right\} \text{ for } p = 1..P \tag{10}$$

This set of nonlinear equations cannot be solved directly and it is necessary to construct a solution using an iterative procedure. The starting point uses the Lewis mapping to obtain the terms $a$, $a_1$ and $a_3$. Both sides of the arbitrarily shaped section are mapped and the values of the parameters averaged. Also substituting the conditions given by equation 9 into equation 10 with $N = 0$ we find that $a_0 = \frac{b_s - b_p}{2}$. These form the basis of the multiparameter mapping which is used to accurately map the section perimeter. To complete the first asymmetric mapping it is necessary to obtain $a_2$. This is achieved using the following procedure

1. A large number of points are defined in the $\zeta$ plane around the perimeter of the semi circular contour, the angles $\theta$ associated with each point are calculated.

2. Using the *current completed* mapping (in the first instance this will be the Lewis mapping plus the $a_0$ term) the points in the $\zeta$ plane are mapped to the $z$ plane.

3. The distance around the *mapped* section girth to each mapped point from the first mapped point (the first mapped point will be the offset on the starboard waterline) is then calculated. This creates a monotonic relationship between the assumed angles $\theta$ in the $\zeta$ plane and the distance around the section girth in the $z$ plane. The advantage of this approach is that the relationship is *always* monotonic no matter what the shape of the section is.

   One popular method to obtain a relationship between the $\zeta$ and $z$ planes involves relating the assumed angles $\theta$ in the $\zeta$ plane to the angles $\phi$ subtended by the mapped points in the $z$ plane. However it is possible in the $z$ plane that one angle $\phi$ may correspond to more than one point on the section perimeter. If this occurs the section may not be mapped. This occurs with sections possessing large bulbous bows. The *line length* method does not suffer from this restriction and in practice almost any shape may be mapped.

4. The distance around the *true* section girth to each *section definition* point from the first section definition point is calculated.

5. Using the relationship established in item 3 the angles $\theta_p$ in the $\zeta$ plane relating to each section definition point may be determined. This is achieved

by interpolating for an angle $\theta_p$ using the line length corresponding to each definition point. The interpolation is completed using the data calculated in item 3.

6. As each definition point has a corresponding angle $\theta_p$ in the $\zeta$ plane the set of simultaneous equations (10) becomes linear, the only unknowns are the transform parameters $a_n$. Increasing the number of unknown parameters by one (in the first instance this will be the $a_2$ term) allows a new set of parameters to be obtained. This is completed using a least square fit to the definition data. The problem in matrix form becomes

$$\boldsymbol{N}\boldsymbol{A} = \boldsymbol{P} \tag{11}$$

where the matrix $\boldsymbol{N}$ is given by

$$\boldsymbol{N} = \begin{bmatrix}
\sin\theta_1 & 1 & \sin\theta_1 & \ldots\ldots & (-1)^n\cos 2n\theta_1 & (-1)^n\sin(2n+1)\theta_1 & \ldots\ldots & (-1)^N\cos 2N\theta_1 & (-1)^N\sin(2N+1)\theta_1 \\
\vdots & & & & \vdots & \vdots & & & \vdots \\
\sin\theta_p & 1 & \sin\theta_p & \ldots\ldots & (-1)^n\cos 2n\theta_p & (-1)^n\sin(2n+1)\theta_p & \ldots\ldots & (-1)^N\cos 2N\theta_p & (-1)^N\sin(2N+1)\theta_p \\
\vdots & & & & \vdots & \vdots & & & \vdots \\
\sin\theta_P & 1 & \sin\theta_P & \ldots\ldots & (-1)^n\cos 2n\theta_P & (-1)^n\sin(2n+1)\theta_P & \ldots\ldots & (-1)^N\cos 2N\theta_P & (-1)^N\sin(2N+1)\theta_P \\
\cos\theta_1 & 0 & -\cos\theta_1 & \ldots\ldots & (-1)^n\sin 2n\theta_1 & -(-1)^n\cos(2n+1)\theta_1 & \ldots\ldots & (-1)^N\sin 2N\theta_1 & -(-1)^N\cos(2N+1)\theta_1 \\
\vdots & & & & \vdots & \vdots & & & \vdots \\
\cos\theta_p & 0 & -\cos\theta_p & \ldots\ldots & (-1)^n\sin 2n\theta_p & -(-1)^n\cos(2n+1)\theta_p & \ldots\ldots & (-1)^N\sin 2N\theta_p & -(-1)^N\cos(2N+1)\theta_p \\
\vdots & & & & \vdots & \vdots & & & \vdots \\
\cos\theta_P & 0 & -\cos\theta_P & \ldots\ldots & (-1)^n\sin 2n\theta_P & -(-1)^n\cos(2n+1)\theta_P & \ldots\ldots & (-1)^N\sin 2N\theta_P & -(-1)^N\cos(2N+1)\theta_P
\end{bmatrix} \tag{12}$$

The matrices $\boldsymbol{A}$ and $\boldsymbol{P}$ are given by

$$\boldsymbol{A} = \begin{bmatrix} a \\ a_0 \\ a_1 \\ \vdots \\ a_{2n} \\ a_{2n+1} \\ \vdots \\ a_{2N} \\ a_{2N+1} \end{bmatrix} \qquad \boldsymbol{P} = \begin{bmatrix} x_1 \\ \vdots \\ x_p \\ \vdots \\ x_P \\ y_1 \\ \vdots \\ y_p \\ \vdots \\ y_P \end{bmatrix} \tag{13}$$

The matrix $\boldsymbol{N}$, in general, is not square and has the order $2P(2N+3)$. To simplify the solution it is appropriate to multiply both sides of equation 11 by the transpose of $\boldsymbol{N}$ written here as $\boldsymbol{N}^T$.

$$\boldsymbol{N}^T\boldsymbol{N}\boldsymbol{A} = \boldsymbol{N}^T\boldsymbol{P} \tag{14}$$

This renders the product $\boldsymbol{N}^T\boldsymbol{N}$ square with the order $(2N+3)^2$. The matrix $\boldsymbol{N}^T\boldsymbol{N}$ has the general form

$$\boldsymbol{N}^T\boldsymbol{N} = \left[\begin{array}{c|cc|c} P & \sum_{p=1}^{p=P}(-1)^{n_2}\sin(2n_2+1)\theta_p & -\sum_{p=1}^{p=P}(-1)^{n_2}\cos 2(n_2+1)\theta_p & \cdots\cdots \\ \hline \sum_{p=1}^{p=P}(-1)^{n_1}\sin(2n_1+1)\theta_p & \sum_{p=1}^{p=P}(-1)^{n_1+n_2}\cos(n_1-n_2)\theta_p & -\sum_{p=1}^{p=P}(-1)^{n_1+n_2}\sin[2(n_1-n_2)-1]\theta_p & \cdots\cdots \\ -\sum_{p=1}^{p=P}(-1)^{n_1}\cos 2(n_1+1)\theta_p & \sum_{p=1}^{p=P}(-1)^{n_1+n_2}\sin[2(n_1-n_2)+1]\theta_p & \sum_{p=1}^{p=P}(-1)^{n_1+n_2}\cos 2(n_1-n_2)\theta_p & \cdots\cdots \\ \vdots & \vdots & \vdots & \cdots\cdots \\ \vdots & \vdots & \vdots & \cdots\cdots \\ \vdots & \vdots & \vdots & \cdots\cdots \\ \vdots & \vdots & \vdots & \cdots\cdots \end{array}\right] \tag{15}$$

The subscripts on the $n$ terms relate to the horizontal line and vertical column indexes. The first line is due to the scale factor $a$ and only appears in the position shown. It is composed of the term $P$ and the following two terms are repeated for different values of $n_2$, $0 \leq n_2 \leq N$. The first column is due to the scale factor $a$ and only appears in the position shown. It is composed of the term $P$ and the following two terms are repeated for different values of $n_1$, $0 \leq n_1 \leq N$. The interior of the matrix is composed of the remaining four terms repeating for various values of $n_1$ and $n_2$. The matrix $\boldsymbol{N}^T\boldsymbol{N}$ is now obviously square. $\boldsymbol{N}^T\boldsymbol{P}$ is given by

$$\boldsymbol{N}^T\boldsymbol{P} = \left[\begin{array}{c} \sum_{p=1}^{p=P} x_p\sin\theta_p + y_p\cos\theta_p \\ \sum_{p=1}^{p=P}(-1)^{n_1}\left[x_p\cos 2n_1\theta_p + y_p\sin 2n_1\theta_p\right] \\ \sum_{p=1}^{p=P}(-1)^{n_1}\left[x_p\sin(2n_1+1)\theta_p - y_p\cos(2n_1+1)\theta_p\right] \\ \vdots \\ \vdots \\ \vdots \\ \vdots \end{array}\right] \tag{16}$$

The first term appears only once, the remainder of the matrix consists of the next two terms repeated for different values of $n_1$, $0 \leq n_1 \leq N$.

The transform parameters can now be easily obtained using a standard technique of matrix inversion.

7. A new set of transform parameters have been obtained using the preceeding method (in the first instance new values for $a$, $a_0$, $a_1$ and $a_3$ are obtained and an initial value for $a_2$ is derived). The process is now repeated until the transformation adequately maps the section definition or an upper limit of N is reached.

Figure 2 illustrates the progression from the Lewis mapping plus the offset parameter $a_0$ (four parameter) to a five parameter mapping. The full line in the

left hand diagram is the section perimeter obtained using the four parameter mapping, the starred points correspond to the section definition points mapped with the current completed mapping. The angles used to map the section definition points are those obtained using the technique described in item 5. The section definition points are indicated by an $\times$. The dotted line is the mapped section perimeter obtained using the derived five parameter mapping. The small circles represent the new positions of the starred points. Note how much the mapped section has changed with the addition of one extra parameter. The diagram on the right hand side illustrates the addition of another parameter, i.e. the dotted line in the left hand diagram has become the full line in the right hand diagram. The dotted line now represents the transformation with six parameters. Successive transformations gradually approach the section definition.

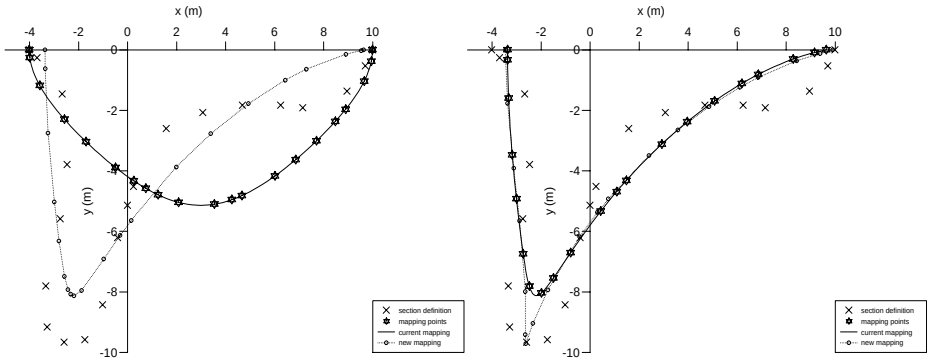


Figure 2: Development of a fine section at $15^o$ using the line length method.

## 2.4 Examples of the multiparameter mapping.

Various sections are considered demonstrating the versatility of the mapping. The definitions and solutions are given for rectangular and fine sections in order that the work is reproducible. Additionally, the solution after each iteration for the rectangular section is detailed. These sections are those used by Bishop et al(1979). Bulbous sections and those possessing bilge keels and shaft brackets are also included.

**Rectangular section.** A rectangular section is outside the range applicable to the Lewis transforms ($\sigma = 1$, $\lambda = 1.5$) as dictated by equation 8 and the first approximation is started on the upper limit of the second inequality. The zero heel section is defined by the coordinates

| | | | | | | | | | |
|---|---|---|---|---|---|---|---|---|---|
| $x$(m) | 7.500 | 7.500 | 7.500 | 3.750 | 0.000 | -3.750 | -7.500 | -7.500 | -7.500 |
| $y$(m) | 0.000 | 3.750 | 7.500 | 7.500 | 7.500 | 7.500 | 7.500 | 3.750 | 0.000 |

Table 1: Offsets for the rectangular section at $0^o$.

and the final mapping using twelve parameters is shown in the left hand diagram of Figure 3.

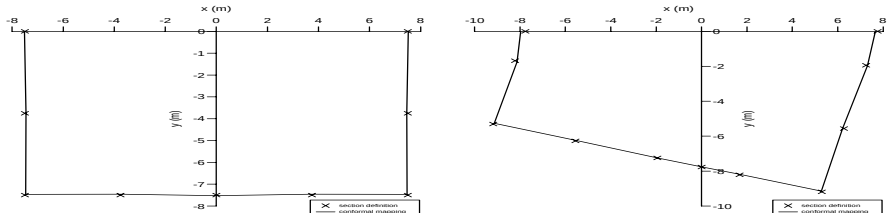


Figure 3: Mappings using 12 transform parameters for a rectangular section at $0^o$ and $15^o$.

The twelve parameter mapping is created using the following sequence of transform parameters

| N | a | $a_0$ | $a_1$ | $a_2$ | $a_3$ | $a_4$ |
|---|---|---|---|---|---|---|
| 1 | 8.781 | -1.520x10$^{-15}$ | 1.723x10$^{-3}$ | 5.618x10$^{-16}$ | -1.338 | - |
| 2 | 8.861 | -4.357x10$^{-15}$ | 3.506x10$^{-3}$ | -3.121x10$^{-16}$ | -1.469 | 1.731x10$^{-15}$ |
| 2 | 8.887 | 1.711x10$^{-16}$ | 3.345x10$^{-3}$ | -7.060x10$^{-16}$ | -1.509 | 9.520x10$^{-16}$ |
| 3 | 8.894 | -5.543x10$^{-16}$ | 3.414x10$^{-3}$ | -1.666x10$^{-16}$ | -1.521 | -3.754x10$^{-16}$ |
| 3 | 8.903 | 3.785x10$^{-15}$ | 1.721x10$^{-3}$ | -2.249x10$^{-15}$ | -1.551 | 1.521x10$^{-15}$ |
| 4 | 8.895 | 1.145x10$^{-15}$ | 5.015x10$^{-4}$ | -8.603x10$^{-16}$ | -1.540 | -2.542x10$^{-18}$ |
| 4 | 8.887 | 3.358x10$^{-15}$ | -2.223x10$^{-4}$ | -2.326x10$^{-15}$ | -1.528 | 1.554x10$^{-15}$ |
| 5 | 8.882 | -3.551x10$^{-16}$ | -5.979x10$^{-4}$ | 3.530x10$^{-16}$ | -1.520 | -6.308x10$^{-16}$ |
| N | | $a_5$ | $a_6$ | $a_7$ | $a_8$ | $a_9$ | $a_{10}$ |
| 1 | | - | - | - | - | - | - |
| 2 | | - | - | - | - | - | - |
| 2 | | 3.368x10$^{-3}$ | - | - | - | - | - |
| 3 | | 5.166x10$^{-3}$ | -6.059x10$^{-17}$ | - | - | - | - |
| 3 | | 4.301x10$^{-3}$ | 3.566x10$^{-16}$ | 9.478x10$^{-2}$ | - | - | - |
| 4 | | 2.610x10$^{-3}$ | -3.898x10$^{-16}$ | 0.135 | 2.471x10$^{-16}$ | - | - |
| 4 | | 1.187x10$^{-3}$ | 2.796x10$^{-16}$ | 0.152 | -1.022x10$^{-16}$ | -4.422x10$^{-4}$ | - |
| 5 | | 2.162x10$^{-4}$ | 2.206x10$^{-16}$ | 0.159 | 6.338x10$^{-16}$ | -8.571x10$^{-4}$ | -6.083x10$^{-17}$ |

Table 2: The transform parameters for the rectangular section at $0^o$.

The even transform parameters have very small values due to the section possessing symmetry, in theory these values should be zero. The coordinates and the angles of the final mapped section are given in Table 3.

| $\theta$(rads) | 1.571 | 1.265 | 0.786 | 0.305 | 0.000 | -0.305 | -0.786 | -1.265 | -1.571 |
|---|---|---|---|---|---|---|---|---|---|
| $x$(m) | 7.520 | 7.461 | 7.467 | 3.740 | 0.000 | -3.740 | -7.467 | -7.461 | -7.520 |
| $y$(m) | 0.000 | 3.742 | 7.468 | 7.460 | 7.523 | 7.460 | 7.468 | 3.742 | 0.000 |

Table 3: Final mapped points for the rectangular section at $0^o$.

It can be seen that the mapping is able to accurately map sharp corners without special consideration, see Landweber and Macagno(1975). The rectangular section rotated about the origin through an angle of $15^o$ is defined by the coordinates

| $x$(m) | 7.765 | 7.244 | 6.274 | 5.303 | 1.681 | 0.000 | -1.941 | -5.563 | -9.186 | -8.215 | -7.765 |
|---|---|---|---|---|---|---|---|---|---|---|---|
| $y$(m) | 0.000 | 1.941 | 5.563 | 9.186 | 8.215 | 7.765 | 7.244 | 6.274 | 5.303 | 1.681 | 0.000 |

Table 4: Offsets for the rectangular section at $15^o$.

The mapping using twelve parameters in shown in the right hand diagram of Figure 3. It can be seen that additional centreline and waterline points have been inserted. These are required at the start of the mapping process when both sides of the asymmetric section are Lewis transformed. The final twelve transform parameters are

| $a$ | $a_0$ | $a_1$ | $a_2$ | $a_3$ | $a_4$ |
|---|---|---|---|---|---|
| 8.854 | -0.358 | -5.222x10$^{-2}$ | -0.877 | -0.875 | 0.763 |
| $a_5$ | $a_6$ | $a_7$ | $a_8$ | $a_9$ | $a_{10}$ |
| -3.496x10$^{-2}$ | 0.291 | -7.135x10$^{-2}$ | 7.969x10$^{-3}$ | -1.109x10$^{-2}$ | 1.551x10$^{-2}$ |

Table 5: Final transform parameters for the rectangular section at $15^o$.

and the coordinates and angles of the final mapped section are given in Table 6.

| $\theta$(rads) | 1.571 | 1.362 | 1.035 | 0.544 | 0.059 | -0.084 | -0.245 | -0.549 | -1.018 | -1.455 | -1.571 |
|---|---|---|---|---|---|---|---|---|---|---|---|
| $x$(m) | 7.652 | 7.315 | 6.213 | 5.271 | 1.666 | -0.011 | -1.931 | -5.550 | -9.136 | -8.130 | -7.967 |
| $y$(m) | 0.000 | 1.962 | 5.555 | 9.145 | 8.184 | 7.756 | 7.252 | 6.241 | 5.262 | 1.750 | 0.000 |

Table 6: Final mapped points for the rectangular section at $15^o$.

**Fine section.** A fine section is also outside the range applicable to the Lewis transforms ($\sigma = 0.252$, $\lambda = 0.74$) and the first approximation is started on the lower limit of the first inequality given in equation 8. The zero heel section is defined by the coordinates

| | | | | | | | | | | |
|---|---|---|---|---|---|---|---|---|---|---|
| $x$(m) | 7.400 | 6.500 | 5.000 | 3.500 | 2.200 | 1.400 | 1.210 | 1.200 | 0.800 | 0.000 |
| $y$(m) | 0.000 | 0.150 | 0.550 | 1.200 | 2.100 | 4.300 | 6.100 | 8.400 | 9.700 | 10.000 |
| $x$(m) | -0.800 | -1.200 | -1.210 | -1.400 | -2.200 | -3.500 | -5.000 | -6.500 | -7.400 | |
| $y$(m) | 9.700 | 8.400 | 6.100 | 4.300 | 2.100 | 1.200 | 0.550 | 0.150 | 0.000 | |

Table 7: Offsets for the fine section at $0^o$.

The mapping for the zero heel section is shown in the left hand diagram of Figure 4.

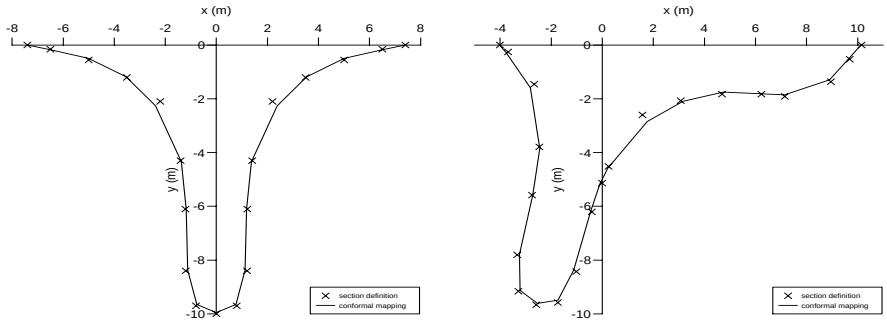


Figure 4: Mappings using 20 transform parameters for a fine section at $0^o$ and $15^o$.

The final twenty transform parameters are

| | | | | |
|---|---|---|---|---|
| $a$<br>6.806 | $a_0$<br>1.675x10$^{-16}$ | $a_1$<br>-2.163 | $a_2$<br>2.731x10$^{-15}$ | $a_3$<br>1.897 |
| $a_4$<br>5.283x10$^{-16}$ | $a_5$<br>1.069 | $a_6$<br>-5.645x10$^{-16}$ | $a_7$<br>3.110x10$^{-2}$ | $a_8$<br>-1.071x10$^{-15}$ |
| $a_9$<br>-0.244 | $a_{10}$<br>2.949x10$^{-16}$ | $a_{11}$<br>-0.143 | $a_{12}$<br>4.176 | $a_{13}$<br>3.213x10$^{-2}$ |
| $a_{14}$<br>-1.972x10$^{-15}$ | $a_{15}$<br>7.884x10$^{-2}$ | $a_{16}$<br>-2.690x10$^{-16}$ | $a_{17}$<br>2.448x10$^{-2}$ | $a_{18}$<br>2.663x10$^{-16}$ |

Table 8: Final transform parameters for the fine section at $0^o$.

Again the even transform parameters are effectively zero because the section is symmetric. The coordinates and the angles of the final mapped section are given by

| | | | | | | | | | | |
|---|---|---|---|---|---|---|---|---|---|---|
| $\theta$(rads) | 1.571 | 1.333 | 1.181 | 1.085 | 1.007 | 0.894 | 0.786 | 0.547 | 0.269 | 0.000 |
| $x$(m) | 7.389 | 6.481 | 5.008 | 3.540 | 2.385 | 1.373 | 1.187 | 1.119 | 0.768 | 0.000 |
| $y$(m) | 0.000 | 0.175 | 0.493 | 1.179 | 2.258 | 4.342 | 6.103 | 8.378 | 9.651 | 9.951 |
| $\theta$(rads) | -0.269 | -0.547 | -0.786 | -0.894 | -1.007 | -1.085 | -1.181 | -1.333 | -1.571 | |
| $x$(m) | -0.768 | -1.119 | -1.187 | -1.373 | -2.385 | -3.540 | -5.008 | -6.481 | -7.389 | |
| $y$(m) | 9.651 | 8.378 | 6.103 | 4.342 | 2.258 | 1.179 | 0.493 | 0.175 | 0.000 | |

Table 9: Final mapped points for the fine section at $0^o$.

It can be seen that using twenty parameters an extremely good mapping may be obtained. The fine section rotated about the origin through an angle of $15^o$ is defined by the coordinates given in Table 10.

| | | | | | | | | | | |
|---|---|---|---|---|---|---|---|---|---|---|
| $x$(m) | 9.986 | 9.694 | 8.952 | 7.148 | 6.240 | 4.687 | 3.070 | 1.582 | 0.239 | 0.000 | -0.410 |
| $y$(m) | 0.000 | 0.527 | 1.363 | 1.915 | 1.827 | 1.825 | 2.065 | 2.598 | 4.516 | 5.139 | 6.205 |
| $x$(m) | -1.015 | -1.738 | -2.588 | -3.283 | -3.333 | -2.748 | -2.465 | -2.669 | -3.691 | -4.011 | |
| $y$(m) | 8.424 | 9.577 | 9.659 | 9.162 | 7.803 | 5.579 | 3.791 | 1.459 | 0.253 | 0.000 | |

Table 10: Offsets for the fine section at $15^o$.

The mapped section is shown in the right hand diagram of Figure 4. The final twenty transform parameters are

| | | | | |
|---|---|---|---|---|
| $a$<br>7.191 | $a_0$<br>0.859 | $a_1$<br>-1.069 | $a_2$<br>2.857 | $a_3$<br>0.689 |
| $a_4$<br>-0.106 | $a_5$<br>-0.434 | $a_6$<br>-0.505 | $a_7$<br>0.186 | $a_8$<br>$8.953\text{x}10^{-2}$ |
| $a_9$<br>0.294 | $a_{10}$<br>$-6.109\text{x}10^{-2}$ | $a_{11}$<br>$3.667\text{x}10^{-3}$ | $a_{12}$<br>-0.160 | $a_{13}$<br>$2.029\text{x}10^{-2}$ |
| $a_{14}$<br>$1.296\text{x}10^{-3}$ | $a_{15}$<br>$9.191\text{x}10^{-2}$ | $a_{16}$<br>$1.891\text{x}10^{-2}$ | $a_{17}$<br>$1.361\text{x}10^{-2}$ | $a_{18}$<br>$-2.552\text{x}10^{-2}$ |

Table 11: Final transform parameters for the fine section at $15^o$.

The coordinates and angles of the final mapped section are given by

| | | | | | | | | | | | |
|---|---|---|---|---|---|---|---|---|---|---|---|
| $\theta$(rads) | 1.571 | 1.401 | 1.170 | 0.907 | 0.819 | 0.725 | 0.651 | 0.586 | 0.488 | 0.456 | 0.394 |
| $x$(m) | 9.981 | 9.632 | 8.920 | 7.131 | 6.260 | 4.731 | 3.148 | 1.769 | 0.216 | -0.093 | -0.480 |
| $y$(m) | 0.000 | 0.498 | 1.270 | 1.870 | 1.796 | 1.741 | 2.106 | 2.866 | 4.575 | 5.154 | 6.204 |
| $\theta$(rads) | 0.181 | -0.069 | -0.324 | -0.591 | -0.871 | -1.114 | -1.236 | -1.371 | -1.496 | -1.571 | |
| $x$(m) | -1.092 | -1.749 | -2.577 | -3.210 | -3.205 | -2.725 | -2.421 | -2.840 | -3.774 | -4.008 | |
| $y$(m) | 8.363 | 9.518 | 9.595 | 9.092 | 7.796 | 5.593 | 3.863 | 1.592 | 0.305 | 0.000 | |

Table 12: Final mapped points for the fine section at $15^o$.

Figure 5 illustrates the variation in the values of the first five transform parameters to a heel angle of $45^o$ for the fine section.

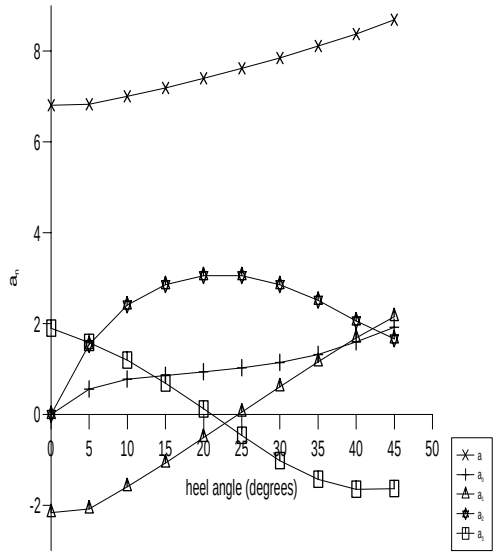


Figure 5: Variation in the first five transform parameters with heel angle for the fine section. Total number of parameters used is 20.

**Bulbous section.** Figure 6 demonstrates that the *line length* method is capable of mapping reentrant sections successfully. At all heel angles the number of parameters used is forty eight. These Figures demonstrate a clear improvement over previous methods.

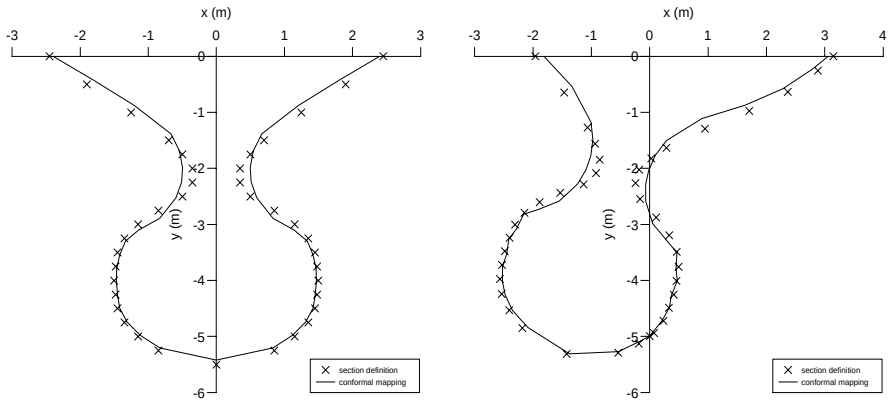


Figure 6: Mappings using 48 transform parameters for a bulbous section at $0^o$ and $15^o$.

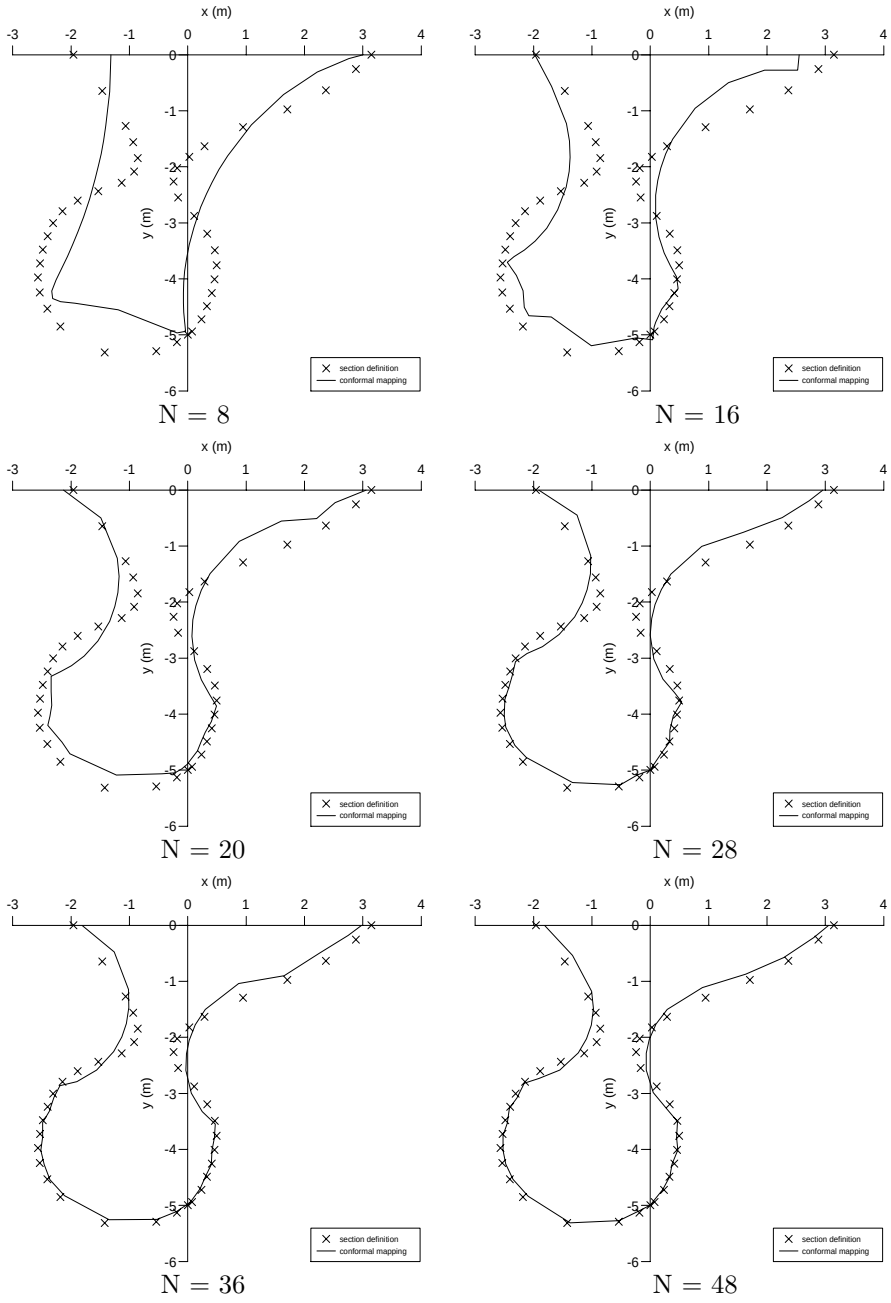


Figure 7: Development of a mapping for a large bulb section at a $15^o$ angle of heel.

Figure 7 illustrates the development of the bulb section at $15^o$. Initially the basic shape is formed, then with an increasing number of parameters the bulb waist reduces. The actual number of parameters used to represent a section is ascertained on a trial and error basis, although, the least square error may provide a numerical indication of the accuracy of the mapping. Use of this figure alone however may result in a poor mapping as it is possible to use too many parameters which will provide an accurate fit at the section definition points but a poor fit between them.

**Other sections.** Figures 8 illustrate a round bilge section including a bilge keel. Figure 9 illustrates the same section with shaft brackets attached. These mapping demonstrate that complicated features can be mapped accurately.

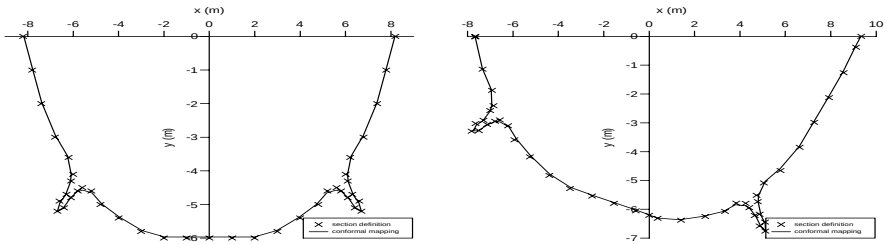


Figure 8: Mappings for a section with bilge keels at $0^o$ and $15^o$.

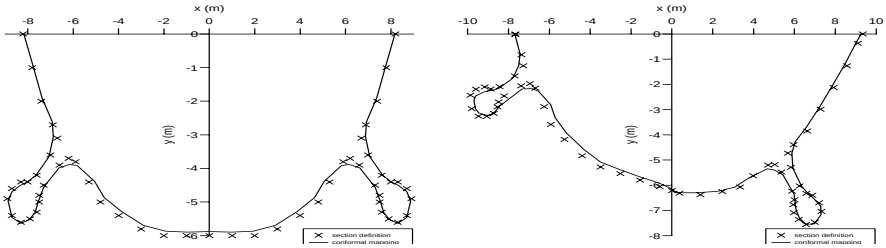


Figure 9: Mappings for a section with shaft brackets at $0^o$ and $15^o$.

# 3 Conclusions.

This new mapping technique provides a simple tool with which sections of arbitrary shape may be conformally mapped to a circle. Using the transform parameters present in the mapping the added mass and damping properties of a section and hence a whole ship may be determined with increased accuracy. The mapping technique may be easily installed in ship motion prediction programs which utilise strip theories.

## Acknowledgement.

This work was supported by the Defence Evaluation and Research Agency.